PLOS ONE

RESEARCH ARTICLE

Gynura procumbens leaf extract-loaded self-microemulsifying drug delivery system offers enhanced protective effects in the hepatorenal organs of the experimental rats

Manik Chandra Shill[1☯], Md. Faisal Bin Jalal[1], Madhabi Lata Shuma[2], Patricia Prova Mollick[1], Md. Abdul Muhit[3], Shimul Halder[4☯*]

1 Department of Pharmaceutical Sciences, North South University, Dhaka, Bangladesh, **2** Department of Pharmacy, School of Pharmacy and Public Health, Independent University Bangladesh, Dhaka, Bangladesh, **3** Department of Clinical Pharmacy and Pharmacology, Faculty of Pharmacy, University of Dhaka, Dhaka, Bangladesh, **4** Department of Pharmaceutical Technology, Faculty of Pharmacy, University of Dhaka, Dhaka, Bangladesh

☯ These authors contributed equally to this work.
* shimulpht@du.ac.bd, manik.shill@northsouth.edu

Citation: Shill MC, Jalal MFB, Shuma ML, Mollick PP, Muhit MA, Halder S (2025) Gynura procumbens leaf extract-loaded self-microemulsifying drug delivery system offers enhanced protective effects in the hepatorenal organs of the experimental rats. PLoS ONE 20(2): e0304435. https://doi.org/10.1371/journal.pone.0304435

Editor: Miquel Vall-llosera Camps, PLOS ONE, UNITED KINGDOM OF GREAT BRITAIN AND NORTHERN IRELAND

Received: May 12, 2024

Accepted: January 29, 2025

Published: February 24, 2025

Data availability statement: All data underlying the findings are within the manuscript.

Funding: The author(s) received no specific funding for this work.

Abstract

Gynura procumbens, known as longevity spinach, is a plant traditionally used in tropical Asian countries for its anti-inflammatory, hepatoprotective, anti-hypertensive, and anti-hyperglycemic properties. The current study aimed to enhance the hepatorenal protective activity of *Gynura procumbens* leaf extract (GLE) by developing a self-microemulsifying drug delivery system (SMEDDS). SMEDDS-GLE exhibited the formation of small micelles with a mean droplet size of 231 nm. This resulted in a significant enhancement in the dispersion of GLE in water, as evidenced by a dispersibility that was at least 4.8 times greater than that of GLE alone. In the rat model of hepatic injury induced by cisplatin (7.5 mg/kg, *i.p.*), the administration of SMEDDS-GLE (75 mg-GLE/kg, *p.o.*) significantly reduced liver damage, observed by histological examination and reduced levels of plasma biomarkers associated with hepatic injury. Furthermore, according to histological examination findings and plasma biomarkers assessment, SMEDDS-GLE enhanced the nephroprotective benefits of GLE in the rat model of acute kidney injury. Based on these findings, a strategic application of the SMEDDS-based approach could be a viable choice to enhance GLE's nutraceutical properties.

1. Introduction

In recent years, there has been a significant rise in the diagnosis of kidney dysfunction, including chronic kidney diseases (CKD), among patients with hepatic illnesses [1]. The growing occurrence of risk factors such as hypertension, diabetes, and nonalcoholic fatty liver disease appears to have had a substantial influence on the increasing occurrence of chronic kidney disease (CKD) [2]. In 2019, the prevalence of chronic kidney disease (CKD) in hospitalized patients with cirrhosis, the final stage of liver disease, has risen to as high as 46.8% [3]. Other

Competing interests: The authors have declared that no competing interests exist.

Abbreviations: ALP, alkaline phosphatase; ALT, alanine aminotransferase; ANOVA, analysis of variance; AST, aspartate aminotransferase; BUN, blood urea nitrogen; CKD, chronic kidney disease; DLS, Dynamic Light Scattering; FT-IR, fourier transform infrared spectroscopy; GLE, *Gynura procumbens* leaves extract; H&E, hematoxylin and eosin; HPLC, high performance liquid chromatography; MCT, medium chain triglyceride; ROS, reactive oxygen species; SMEDDS, self-emulsifying drug delivery system; TEM, transmission electron microscopy; UV, ultraviolet; ZP, zeta potential.

metabolic risk factors such as obesity, hypertension, and prolonged use of synthetic medicines may be coming together to form a notable epidemiological trend, which may exert the growing prevalence of chronic kidney disease (CKD) among patients with cirrhosis [4]. Reactive oxygen species (ROS) are significant contributors to pathological alterations in the liver and kidney. Polyunsaturated fatty acids of biological membranes are highly susceptible to the impact of reactive oxygen species (ROS) for lipid peroxidations. Various innate defensive mechanisms have been evolved to restrict the presence of (ROS) and mitigate their detrimental effects [5,6]. Nevertheless, due to the possibility of incomplete protection or excessive generation of reactive oxygen species (ROS), the inclusion of dietary antioxidants as supplementary protective mechanisms becomes highly significant [7,8]. As a result, numerous natural and synthetic substances with antioxidant characteristics have been suggested as potential treatments for liver diseases caused by oxidative stress [9,10].

The growing belief that medications derived from natural sources, especially those obtained from food, are more reliable and secure has led to a substantial rise in demand for such goods in the nutraceuticals industry [11,12]. Functional foods exert therapeutic effects by selectively suppressing the overexpression of proteins, enzymes, amino acids, and hormones through several pathways [13]. Herbal remedies are gaining popularity in developing and developed nations since they are affordable and have little adverse effects. The World Health Organization (WHO) prioritizes the assessment of secondary metabolites obtained from natural sources for treating diseases, as they have a wide range of effectiveness [14]. Approximately 80% of the population in the lower income countries relies on natural products to meet their main healthcare requirements. Medicinal herbs are rich sources of exogenous antioxidants, which could be a promising alternative for mitigating pathogenic alterations in oxidative stress-related diseases [15]. They have been linked to the treatment of liver damage, diabetes, kidney toxicity, cancer, cardiovascular problems, neurological disorders, inflammation, and the aging process. However, the pharmacological potential of these substances may be impeded by their low water solubility, poor dispersibility in the gastrointestinal tract, low stability, poor absorption, and quick metabolism, resulting in a low therapeutic index [16,17]. Thus, it is inherently challenging to integrate and manage these nutraceuticals within the body for optimum outcomes.

Longevity spinach, scientifically known as *Gynura procumbens*, is a widely recognized traditional food and herb belonging to the Asteraceae family and is commonly used and highly valued in Southeast Asia. *Gynura procumbens* is a plant whose fresh leaves can be consumed raw or cooked [18]. Multiple reports have demonstrated that *Gynura procumbens* Leaves extract (GLE) contains a variety of secondary metabolites, including quercetin, gallic acid, kaempferol, kaempferol-3-O-β-D-glucopyranoside, kaempferol-3-O-rutinoside, rutin, chlorogenic acid, protocatechuic acid, vanillic acid, syringic acid, caffeic acid, p-coumaric acid, ferulic acid, 3,5-dicafeoylquinate methyl ester, terpenoids, tannins, alkaloids, saponins, and astragali [19,20]. In addition, it possesses a diverse array of pharmacological actions, including antihyperglycemic, antihyperlipidemic, antioxidant, organ-protective, antibacterial, and anti-inflammatory activity. It is also used for the treatment of hepatotoxicity and alcohol-induced liver disease [21,22]. Many active components (terpenoids, steroids) found in herbal extracts cannot pass through the lipid barrier because they have a high molecular size and low solubility in water [23]. As a result, they are poorly absorbed into the body and have limited bioavailability. Nanotechnology has lately emerged as an innovative method to tackle the challenges related to the solubility and bioavailability of medications with low water solubility [19,24]. Several innovative drug delivery methods, such as polymeric nanoparticles, liposomes, nanoemulsions, and phytosomes, have been documented for plant extracts and their bioactive components [25,26]. Self-microemulsifying formulation improves the absorption of

phytomolecules with low solubility [27,28]. This is achieved by exploiting their lipidic nature and small particle size. A self-microemulsifying drug delivery system (SMEDDS) combines water-insoluble phytoextract, oil or lipid, surfactant, and cosurfactant. Upon being taken orally, they are mixed with water-based fluids in the gastrointestinal tract (GIT) and create a microemulsion/nanoemulsion with droplets ranging in size from 100 to 500 nanometers [29]. The microemulsion is designed to dissolve the phytomolecules necessary to absorb, which are not readily soluble in water. In addition, the lipid excipients in the self-microemulsifying formulation enhance the transportation of phytomolecules through the lymphatic system, improving bioavailability by reducing the effects of first-pass metabolism. The intracellular concentration of phytomolecules increases due to the weakening of the lipid and surfactant employed by the *P*-glycoprotein efflux mechanism [30]. By boosting the biopharmaceutical properties and enhancing the stability of the gastrointestinal system, the employment of the SMEDDS-based method may help overcome the challenges associated with giving GLE in clinical settings. Therefore, the objective of the present study is to create, analyze, and assess SMEDDS for the oral administration of GLE. The purpose is to enhance the biopharmaceutical properties of GLE, leading to improved hepatoprotective and nephroprotective effects.

2. Materials and methods

2.1. Chemicals and reagents

BASF, Dhaka, Bangladesh graciously gave Kolliphor® P188 and medium chain triglyceride (MCT). Silymarin and Cisplatin were bought from Sigma-Aldrich (St. Louis, MO, USA). Throughout the experiment, all other reagents and solvents were of analytical grade and were acquired from commercial sources.

2.2. Collection, identification, and extraction of plant materials

The National Herbarium in Mirpur, Bangladesh, identified and verified *Gynura procumbens* leaves collected from Natore, Bangladesh. A voucher specimen (DACB accession number: 45273) was recorded at the herbarium. After gathering the leaves, they were carefully cleaned, dried in the shade, and powdered into a fine powder. The leaf powder was soaked in ethanol, thoroughly agitated, filtered, and dried to a crude extract using a rotary evaporator as described in our previous study [31]. To use later, the extract was kept in an airtight falcon tube and refrigerated at 2 to 8 °C.

2.3. HPLC detection and quantification of polyphenolic compounds

The study of specific phenolic components in the ethanol leaf extract of *Gynura procumbens* was carried out using HPLC-DAD detection and quantification techniques. A Dionex UltiMate 3000 system with a photodiode array detector (DAD-3000RS) and quaternary rapid separation pump (LPG-3400RS) was used. An Acclaim® C18 (5 μm) Dionex column (4.6 × 250 mm) at 30 °C, 1 mL/min flow rate using gradient elution mode, and 20 μL injection volume were used to achieve separation. Acetic acid solution pH 3.0 (solvent B), methanol (solvent C), and acetonitrile (solvent A) made up the mobile phase. The detector was calibrated to measure 280 nm for 25.0 min, then 320 nm for 32.0 min, 280 nm for 3 min, and 380 nm for 35 min. The diode array detector was set to an acquisition range of 200 to 700 nm and maintained for the remainder of the analysis. A standard stock solution was made in methanol to create calibration curves. It contained the following: kaempferol (6 μg/mL), pyrogallol, rutin hydrate (12 μg/mL), p-coumaric acid (3 μg/mL), ellagic acid (48 μg/mL each), vanillin, trans-ferulic acid (+)-catechin hydrate, (-)-epicatechin (10 μg/mL each), and

quercetin hydrate (QU) (4 μg/mL). The extract was dissolved in ethanol at a 30 mg/mL concentration. Before HPLC analysis, all solutions mixed standard, sample, and spiked solutions were degassed in an ultrasonic bath (Soner 210H, Rocker Scientific, Taiwan) for 15 min after being filtered through a 0.22 μm syringe filter (Sartorius, Germany). Dionex Chromeleon software was used to calculate data acquisition, peak integration, and calibrations (Version 6.80 RS 10) [31].

2.4. Preparation of pseudo-ternary phase diagram

Using the water titration method, the pseudo-ternary phase diagrams of oil, surfactant, and co-surfactant were created. The oil, surfactant, and co-surfactant mixtures at different weight ratios were combined with water drop-wise, and the resulting emulsion formation was assessed immediately. The mixtures were then gently shaken with water, and the dispersibility, phase clarity, flowability, and precipitation rate were visually evaluated. Following phase diagram validation of the fine emulsion region, the appropriate oil, surfactant, and co-surfactant ratio was chosen for further physicochemical and pharmacodynamic analyses. Based on the observed data, the pseudo-ternary phase diagram was produced using SigmaPlot V14 (Systat Software Inc., UK)

2.5. Formulation of SMEDDS-GLE

By combining the optimized ratio of oil, surfactant, and co-surfactant with the amount of GLE (5%, w/v), SMEDDS-GLE was made. In summary, oil, surfactant, and co-surfactant were accurately measured in glass vials, mixed by inverting, and then heated in a water bath at 37 °C while stirring moderately. The ultimate blend was agitated using a vortex mixer until a transparent solution was achieved. Before being used, the resulting mixture was kept at room temperature in an amber glass bottle.

2.6. Interaction of GLE with polymers

The compatibility and potential interactions between the components of SMEDDS-GLE were assessed by Attenuated Total Reflectance-Fourier Transform Infrared (ATR-FTIR) analysis using a Shimadzu IR-Prestige-21-FT-IR infrared spectrometer (Tokyo, Japan) connected to a horizontal Golden Gate MKII single-reflection ATR system (Specac, Kent, UK). Each sample was placed separately on the instrument's sample platform. For each spectrum, 64 consecutive scans were collected in the 600–4000 cm^{-1} (with a resolution of 4 cm^{-1}). The final spectrum was generated by averaging these observations. The IRsolution 1.30 software (Shimadzu, Tokyo, Japan) was used for all spectral analyses. During the analysis, the baseline of each sample was normalized and corrected.

2.7. Dynamic Light Scattering (DLS)

Using a Malvern Zetasizer Ultra (Malvern Instruments Ltd, Malvern, UK), the DLS method was used to assess the mean particle size, polydispersity index (PDI), and zeta potential of SMEDDS-GLE samples suspended in water at 25 °C and a measuring angle of 90°. After being ten-fold diluted with Milli-Q water, the samples were used to calculate the zeta potential and size distribution. Three replicates of each measurement were carried out.

2.8. Transmission Electron Microscopy (TEM)

Using TEM, the droplets of the optimized SMEDDS-GLE formulation were investigated. In particular, SMEDDS-GLE was poured onto a 300-mesh copper grid coated with carbon after

being diluted 400 times with Milli-Q water (0.5%, w/v). Using Milli-Q water, excess phosphotungstic acid (PTA) was eliminated following negative staining with a 2% (w/v) PTA solution. After that, the copper grid was put in an oven to remove all traces of moisture through vacuum drying. At a voltage of 200 kV, the dried grid was examined using TEM equipment (F200X Talos, Thermo Fisher, Waltham, MA, USA). The droplet size was verified using ImageJ (National Institutes of Health, Bethesda, MD, USA).

2.9. *In vitro* dissolution/dispersion tests

A study assessed the initial self-emulsifying ability of GLE samples (1 g-GLE) by *in vitro* dissolution/dispersion testing. The study employed the USP Type-II dissolution test apparatus, distilled water, and a pH 1.2 (0.1N HCl) solution as the testing mediums. The dispersion test was conducted for 60 min in 900 mL of the media at 37 ± 0.5°C, with continuous stirring at a speed of 50 rpm. Subsequently, the samples were extracted from the central location of the dissolving vessel at specified time intervals (5, 15, 30, 45, and 60 min) using a micropipette. Following each sampling, an equivalent volume of fresh media has been added to the vessel. Subsequently, the sample was centrifugated at 10,000 × *g* for 10 min. The resulting mixture was then passed through a 0.45 μm membrane filter (Millex LG, Millipore, Billerica, MA) and diluted with methanol. The UV spectrophotometer was used to analyze the amounts of dispersed or dissolved GLE at a wavelength of 254 nm [32].

2.10. Animals

Locally bred healthy Wistar albino rats (male rats, body weight within 250 – 300 g) were obtained from North South University, Dhaka, Bangladesh, and kept in pairs in cages. They had unrestricted access to food and water and were subjected to a 12 h cycle of darkness and light. The environment was maintained at a controlled temperature of 24 ± 1 °C and humidity of 55 ± 5% RH. Before the oral delivery of GLE samples, the rats underwent a period of food deprivation lasting at least 12 h, excluding water. All animal-related procedures in this study were carried out per the guidelines approved by the Institutional Animal Care and Ethical Committee of the Faculty of Biological Sciences, University of Dhaka (Approval No. 233, 30 August 2023). In addition, our experiments also adhered to the International Council for Laboratory Animal Science, the Nuffield Council on Bioethics (NCB), and the Council for International Organization of Medical Sciences (CIOMS/ICLAS) guidelines.

2.11. Experimental rat model of Kidney and Liver Injury

We have conducted a study on the acute kidney and liver injury induced by cisplatin (7.5mg/kg) [33], and the nephroprotective and hepatoprotective properties of GLE samples were assessed. Rats were randomly divided into six groups, each with six rats: group I was the control group (received saline); Group II was the negative control group (received GLE only); Group III was the disease group (received cisplatin); Group IV was the GLE treatment group (received cisplatin and GLE); group V was the SMEDDS-GLE treatment group (received cisplatin and SMEDDS-GLE); and Group VI was the positive control group (received cisplatin and silymarin (100 mg/kg)) [34]. The sample size was determined using the power equation while maintaining a 90% power and an E value between 10 and 20. Our study limited the analysis to 4 to 6 rats per group and reduced and refined the experimental animals per NCB and CIOMS/ICLAS guidelines based on the power calculation [35]. In Groups II, IV, V, and VI, rats received an intraperitoneal injection (IP) of cisplatin (7.5 mg/kg dissolved in saline) on the 7th day to induce acute liver and kidney injury. The dose of GLE and SMEDDS-GLE was 75 mg/kg to assess the nephroprotective and hepatoprotective effects based on the findings of

exploratory tests based on earlier reports [31]. After 10 days of treatment, rats were anesthetized using ketamine (100 mg/kg), blood samples were collected, centrifuged at 8,000 × g for 10 min, and plasma was refrigerated at -80 °C until analysis. The rats were euthanized using ketamine (300 mg/kg) and sacrificed to collect kidney and liver tissues. The collected tissues were rinsed with ice-cold saline, dried with filter paper, and well-preserved (10% neutral formalin) for further analysis.

2.12. Evaluation of plasma biochemical markers

BUN and creatinine levels were assessed as indicators of nephrotoxicity using LiquiUV diagnostic kits, a commercially available test kit (HUMAN GmbH, Germany). Following the manufacturer's instructions, the creatinine and BUN levels in plasma were measured spectrophotometrically at 520 and 340 nm using a microplate reader (Safire, Tecan, Männedorf, Switzerland). Moreover, the Fortress diagnostic kit (UK) was used to measure the plasma levels of alkaline phosphatase (ALP), aspartate aminotransferase (AST), and alanine aminotransferase (ALT) as markers of liver impairment. The ALT and AST levels were measured spectrophotometrically at a wavelength of 340 nm. Every sample was assessed three times.

2.13. Histopathological examination of liver and kidney

The liver and kidney tissues were subjected to histological scanning following the methodology described by Quaresma et al. with slight modifications [36]. The collected tissues were then preserved in 10% neutral buffered formalin. The fixed tissues were rinsed three times with phosphate-buffered saline (PBS, pH 7.4) and then placed in a solution of 30% sucrose and 0.1% sodium azide at 4 °C for 24 h. The kidney and liver tissues were sliced into sections with a thickness of 5 μm using a rotary microtome and preserved in paraffin wax. Hematoxylin and eosin (H&E) staining was used to investigate the morphology of the liver and kidney tissues and the presence of inflammatory cell infiltration to evaluate the severity of tissue damage. Subsequently, the sections were carefully investigated, recorded, and photographed using a Zeiss Axioscope 40-X light microscope. Using a previously established procedure, the density of inflammation in the liver and kidney was quantified using ImageJ software (NIH, USA) [37].

2.14. Data analysis

The findings are presented as the mean ± standard error of the mean (SEM). The data was subjected to a one-way analysis of variance (ANOVA) using GraphPad Prism-6 software (San Diego, California, USA) to confirm its statistical significance. Statistical differences were considered significant at a $p \leq 0.05$.

3. Results and discussion

3.1. Characterization of polyphenolic compounds in the ethanolic leaf extract of *gynura procumbens*

The phenolic phytochemicals in the ethanolic leaf extract of *Gynura procumbens* were detected and measured using HPLC. **Fig 1** displays the chromatographic separations of polyphenols in *Gynura procumbens*. The findings of the investigation on the phenolic chemical found in GLE are shown in **Table 1**. The quantities were determined using the relevant calibration curve and presented as the three measurements' averages.

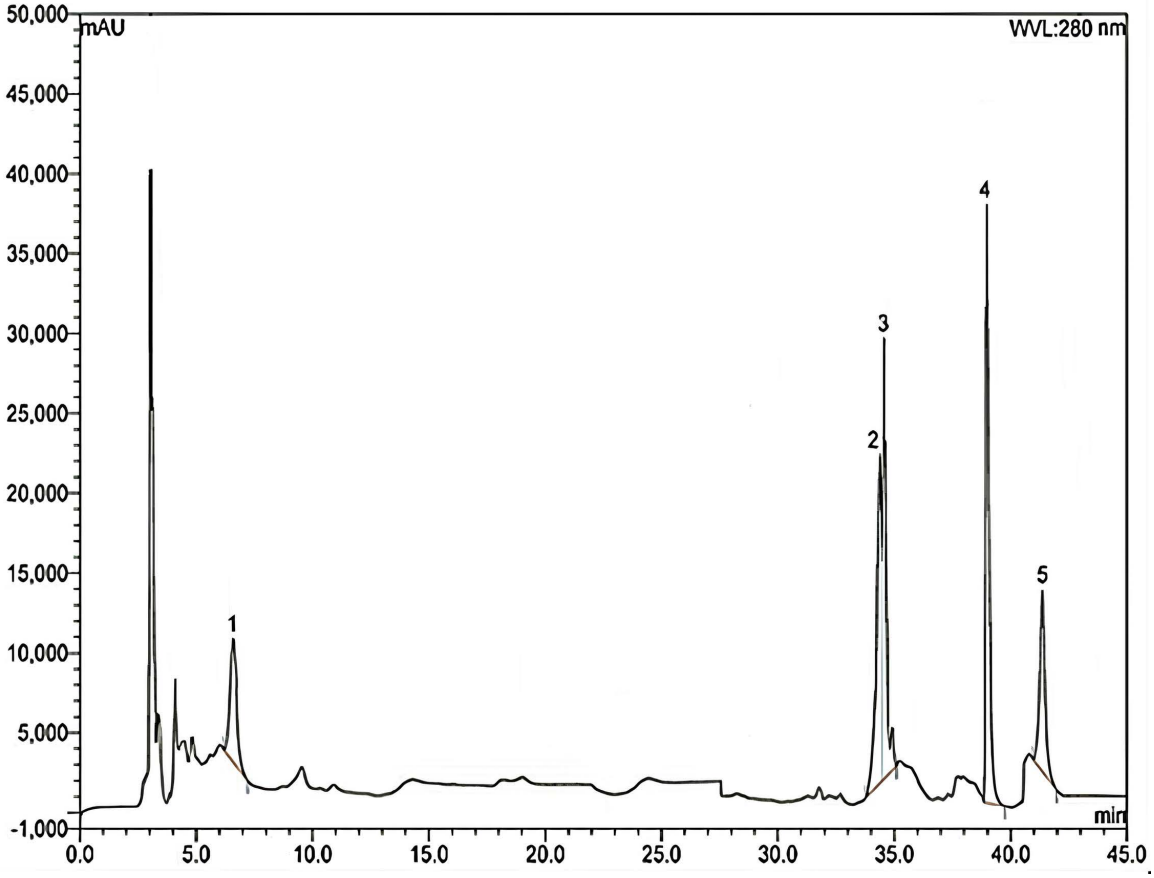

Fig 1. HPLC chromatogram of the ethanolic extract of *Gynura procumbens* [corresponding peaks: 1, gallic acid; 2, ellagic acid; 3, rutin hydrate; 4, quercetin hydrate; 5, kaempferol].

https://doi.org/10.1371/journal.pone.0304435.g001

Table 1. Polyphenolic compounds identified in the ethanol leaf extract of *G. procumbens*.

Polyphenolic compounds	Ethanolic extract of *Gynura procumbens*	
	Content (mg/100 g of dry extract)	%RSD
Gallic acid	10.24	0.38
Ellagic acid	22.09	0.54
Rutin hydrate	40.52	0.71
Quercetin hydrate	58.27	0.92
Kaempferol	13.48	0.47

RSD: Relative standard deviation (n = 3).

https://doi.org/10.1371/journal.pone.0304435.t001

3.2. Optimization of SMEDDS composition

SMEDDS containing oil, surfactant, and co-surfactant are monophasic liquids at room temperature; however, when mixed with water, they form a fine oil-in-water emulsion upon gentle stirring. The solubility of the target molecules in these components is critical for creating a clear, monophasic liquid at room temperature and maintaining it solubilized. Emulsification depends on oil, water, surfactant, and cosurfactant/cosolvent proportions. A ternary diagram is employed to determine the existence of distinct regions within a nanoemulsion.

The symmetrical triangle visually represents the proportions of the three components through graphical delineation. When constructing a ternary phase diagram, three different forms of phages are usually observed: fine microemulsion (transparent nature), coarse emulsion (unstable, milky white), and liquid crystal (translucent gel-like state) [38]. In the absence of GLE, pseudo-ternary phase diagrams (PTPD) were used to locate self-emulsifying regions and optimize SMEDDS' oil, surfactant, and cosurfactant concentrations. The PTPD determines the correct oil, surfactant, and cosurfactant/cosolvent ratio for emulsion with varying water volumes. Different ratios of oil, surfactant, and co-surfactant containing SMEDDS were created, and spontaneous self-emulsification was visually inspected to determine the fine emulsion areas and optimize the ratios (Fig 2). The isotropic mixture of oil, surfactant, and co-surfactant creates an O/W emulsion in water when gently stirred. The change in entropy favors dispersion more than the energy needed to increase its surface area, causing self-emulsification. Oil facilitates medication transport across the intestinal lymphatic system, improving absorption and bioavailability in SMEDDS. In the filled area of Fig 2, transparent microemulsions with the greatest oil solubilization appeared. Since maximal amounts of oil were solubilized with surfactant in this location, it is possible that a reduced interfacial tension between the oil and water phases triggered the formation of the greatest microemulsion in this region. Moreover, large oil phase solubilization occurs by the optimal amount of surfactant and cosurfactant blending.

Additionally, oil-phase fatty acids can affect self-emulsifying system features. Short-chain triglyceride (SCT) or medium-chain triglyceride (MCT) oils also help in nanoemulsion formation. For SMEDDS oil phases, a fine drug solubilizing oil is recommended to maximize target compound loading and prevent drug precipitation following dispersion. Additionally, MCT

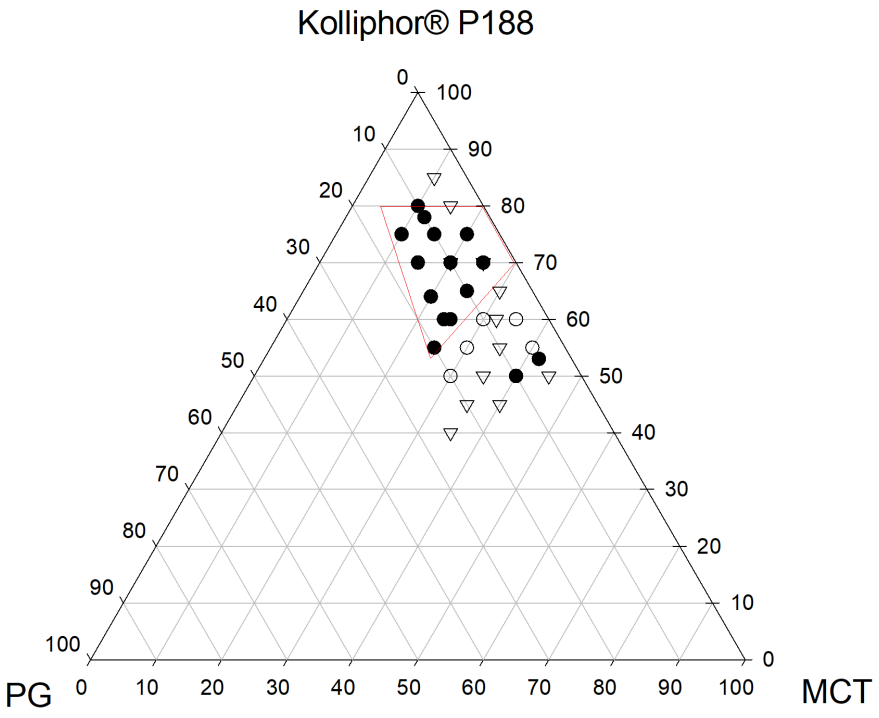

Fig 2. Pseudo-ternary phase diagram of GLE microemulsions in water. KP, Kolliphor® P188 (Surfactant); MCT, medium chain triglyceride (oil); PG, propylene glycol (Co-surfactant); and GLE, *Gynura procumbens* Extract. ● (filled area), fine emulsion region; ▽, coarse emulsion region; and ○, poor or not emulsified.

https://doi.org/10.1371/journal.pone.0304435.g002

exhibits superior emulsification compared to long-chain glycerides. The study utilized Kolliphor® P188, a non-ionic amphiphilic surfactant licensed for pharmaceutical and food usage, due to its low toxicity (LD_{50} = 9380 mg/kg in a rat study) and ability to stabilize emulsions [39]. It was found that at least 50% w/w Kolliphor® P188 was needed to disperse lipids and generate fine emulsion [40]. According to research findings, co-surfactants are crucial components in SMEDDS formulations that boost target compound loading and enlarge the self-emulsification zone in phase diagrams [41]. A single surfactant rarely provides the fluid interfacial film, and microemulsion stability requires brief negative interfacial tension [42]. Co-surfactants usually reduce interface bending stress and give the interfacial layer enough elasticity/flexibility to generate microemulsions in various compositions. This investigation used propylene glycol (PG) as a co-surfactant to stabilize emulsions and finely solubilize GLE. PG is an approved food excipient commonly utilized in nutraceutical formulations due to its low toxicity (LD_{50} = 44 g/kg in rat, oral) [43]. As a co-surfactant, PG might enhance dispersibility by lowering oil-water interfacial tension, potentially accelerating drug absorption in the gastrointestinal system. Increasing surfactant concentration improved self-emulsification, but surfactant concentrations below 50% resulted in poor emulsification, as previously observed. Increasing surfactant concentration stabilizes the oil-water interface, forming a thin, low-viscosity emulsion with microscopic droplets. Higher doses of surfactant and co-surfactant stabilize emulsions with lower globule diameters, resulting in finer emulsions. To minimize toxicity and tissue simulation potential, minimal amounts of surfactant and co-surfactant were selected in formulations for *in vivo* use. A 20:65:15 ratio of oil, surfactant, and co-surfactant was chosen for optimal SMEDDS formulation of GLE and for physicochemical and *in vivo* assessments.

3.3. Physicochemical characterizations of SMEDDS-GLE

The efficiency of fine self-emulsification is strongly dependent on droplet size upon exposure to aqueous media to form fine submicron dispersion, and the stability of SMEDDS varies on droplet size distribution according to the liquid formulation classification system, type-III [44]. DLS analysis (Fig 3A) and TEM observation (Fig 3B) were used to characterize the emulsification property of SMEDDS-GLE products. DLS data showed fine emulsion droplets with an average particle size of about 231 nm and a polydispersity index (PDI) of 0.12 following the dispersion of SMEDDS-GLE in water. Moreover, TEM analyses demonstrated that SEDDS-GLE dispersed in distilled water exhibited a homogeneous and spherical morphology with minimal aggregation. The self-emulsified GLE exhibited a negative surface charge, as indicated by a zeta potential of approximately -48.9 mV. This negative charge could be attributed to free fatty acids on the surface of emulsions derived from MCT, which may prevent particle aggregations due to the electric repulsion between particles [45]. As per a prior study, colloidal dispersions exhibit favorable stability when their zeta potential is high and negative, exceeding −20 mV [46]. This is because of the electric repulsion between the particles. The great colloidal stability of the formulation was also demonstrated when SMEDDS-GLE was dispersed in several aqueous media, such as water, SGF, and SIF, at room temperature, and at least three hours later, no discernible changes in the particle size or zeta potential occurred. The particle sizes observed in the DLS and TEM inspections exhibited a slight disparity. The variations in size observed between the DLS and TEM results can be attributable to the variation in measuring technique. DLS measures the hydrodynamic radius influenced by angle-dependent phenomena, while TEM analysis is conducted on dehydrated samples where the corona is squeezed onto the surface of the droplet [47]. The results suggest that the SMEDDS-GLE exhibited a very limited range of particle sizes and excellent ability to disperse, potentially enhancing the oral absorption and dissolution properties of GLE.

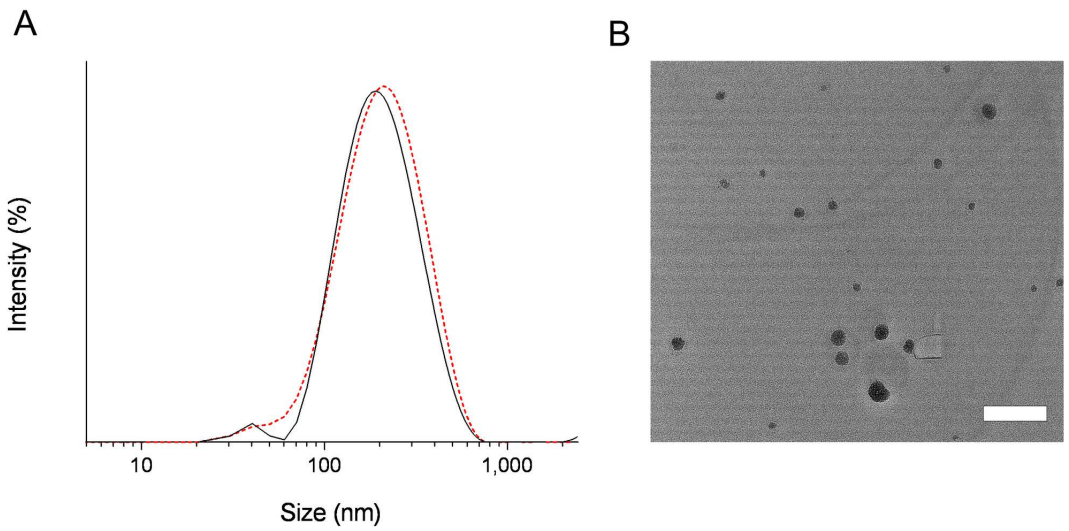

Fig 3. Micelle forming potency of GLE samples dispersed in water. (A) DLS analysis determined the emulsion size distribution of SMEDDS-GLE spread in distilled water: The solid line represents the micelle size distribution at 0 min after dispersion, and the dotted line represents the micelle size distribution at 3 h after dispersion. (B) TEM image of SMEDDS-GLE dispersed in distilled water. Bar represents 200 nm.

https://doi.org/10.1371/journal.pone.0304435.g003

3.4. *In vitro* dispersion/dissolution test of SMEDDS-GLE

Bioactive plant extracts frequently possess several chemical compounds characterized by solubility and stability profiles dependent on pH levels. Acidic conditions can affect these bioactive plant extracts' stability and release rate from nanoparticles. Testing under these conditions demonstrates how the nanoparticles protect or progressively release the plant extract, providing insights into their efficacy. The dissolution/dispersion behaviour of GLE samples is shown in Fig 4 Improved clinical outcomes are indicated by increased dissolution/dispersion, which indicates a higher dissolving rate followed by higher absorption. Poor GLE dispersion was indicated by the 18.8% dissolution/dispersion in water after 60 min.

On the other hand, at least 4.8-fold better dissolution/dispersion behaviour was seen in SMEDDS-GLE, suggesting fine emulsification (Fig 4A). However, in an acidic environment, GLE showed poor dissolution/dispersion behaviour, with 13.3% of the GLE dispersed after 60 min. In contrast, SMEDDS-GLE showed better dispersion, increasing by 7-fold after 60 min before plateauing (Fig 4B). Rapid GLE dissolving and dispersion behaviours in SMEDDS-GLE could be demonstrated from the dissolution/dispersion behaviour data, and this SMEDDS-GLE technique would accelerate the high and quick oral absorption of GLE's active ingredients. The dissolution rate of the SMEDDS was significantly enhanced by the reduced particle size and enlarged surface area of the emulsion droplets. Including surface stabilizers in plant, extract enhances the solubility and wettability of poorly soluble flavonoids in the dissolving medium. This, in turn, contributes to the faster dissolution rate of SMEDDS-GLE.

3.5. Interaction among SMEDDS-GLE components using FTIR-ATR analysis

The FTIR-ATR study was conducted to determine the possible interaction between the components of SMEDDS and GLE. GLE is known for its abundance of quercetin, gallic acid, kaempferol, rutin, chlorogenic acid, protocatechuic acid, vanillic acid, syringic acid, caffeic

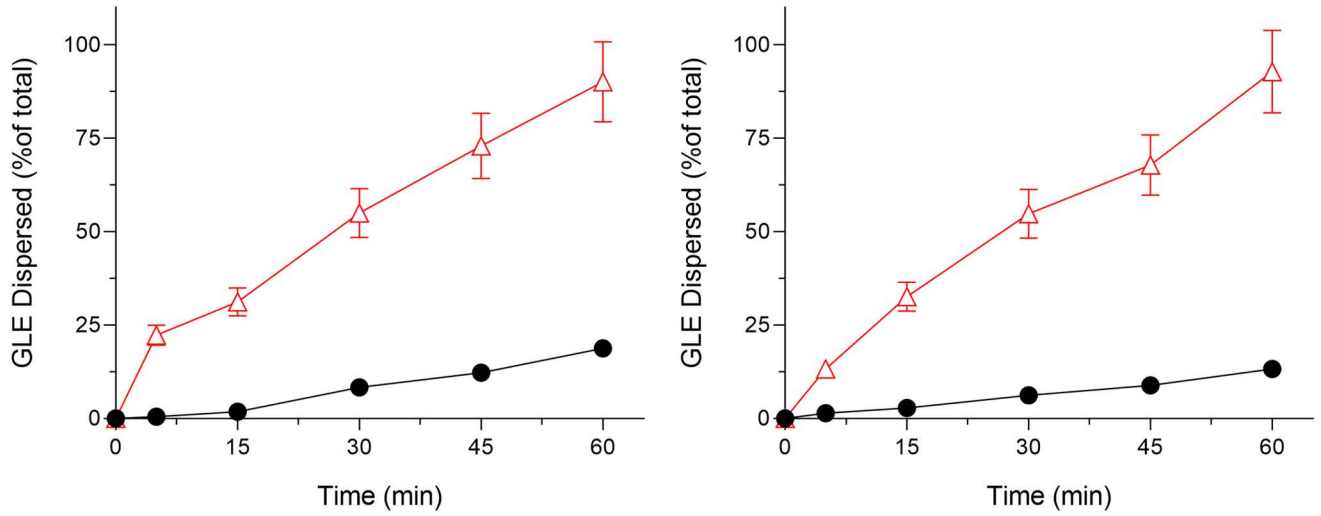

Fig 4. Dissolution/dispersion tests of GLE samples (A) Dissolution/dispersion tests in distilled water; (B) Dissolution/dispersion tests under acidic conditions (0.1 N HCl, pH 1.2). ●, GLE and △, SMEDDS-GLE. Each bar represents the mean ± S.D. of 3 independent experiments.

https://doi.org/10.1371/journal.pone.0304435.g004

acid, p-coumaric acid, and ferulic acid, which are believed to contribute to its pharmacological effects. The FTIR spectra analysis has identified a variety of distinct peaks that can be attributed to different functional groups, such as C-H, -CH_2, -CH_3, C = O, and C = C (Fig 5). The spectra of GLE showed distinct absorption bands at 1370 and 1167 cm^{-1}, indicating the presence of C-H bending and C-O stretching groups in the GLE. Furthermore, the presence of methyl and isopropyl substituents is indicated by the two strong bands seen at 2,923 cm^{-1} and 2,853.6 cm^{-1}, which can be attributed to the stretching of C-H bonds in an aliphatic group. Additionally, a significant and distinct band is detected at 1,743.7 cm^{-1}, indicating the presence of the ketone group through stretching the C = O bond. The two additional peaks observed at 1,463.8 and 1,377.5 cm^{-1} can be attributed to the absorption of C-H bonds in a scissoring motion and the vibration of methyl groups, respectively. However, there was a small change in the bands in the C = O region (1,650–1,750 cm^{-1}) in SMEDDS-GLE.

Furthermore, in the SMEDDS-GLE system, the spectra exhibited a faint and widened peak in the C-H stretching region, attributed to the hydrophobic interaction. The results of the FT-IR spectrum analyses suggest a modest conformational transformation in the spectra, indicating that GLE was dispersed in SMEDDS. As observed in previous studies, this dispersion led to enhanced dissolution and dispersion behaviour [48,49].

3.6. Hepatoprotective effects of SMEDDS-GLE

Multiple published studies have shown that natural antioxidants, such as polyphenols, are powerful bioactive antioxidants that disrupt lipid peroxidation chains by neutralizing highly reactive oxygen radicals. Studies have demonstrated that GLE can enhance the levels of hepatic endogenous antioxidant enzymes such as superoxide dismutase and catalase. This effect may be beneficial in protecting against oxidative diseases caused by free radicals. The study found that SMEDDS-GLE enhanced the biopharmaceutical properties of GLE. As a result, SMEDDS-GLE may demonstrate enhanced hepatoprotective benefits against hepatic injury induced by cisplatin in rats. Plasma ALT, AST, and ALP values as surrogate biomarkers were considered to assess hepatotoxicity and evaluate hepatocellular damage in a rat model treated with cisplatin. The findings demonstrated a significant increase in ALT, AST, and ALP

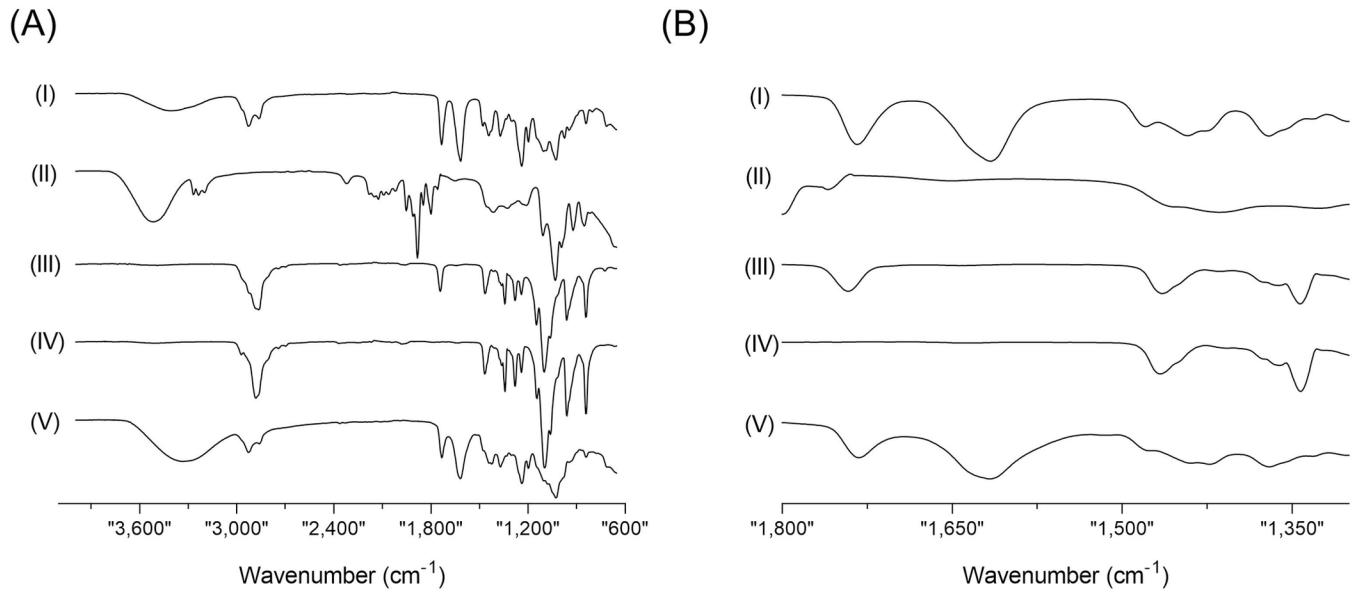

Fig 5. ATR-FTIR spectroscopic analysis of GLE samples in the spectral region from (A) 4,000–600 cm^{-1} and (B) 1,800–1,300 cm^{-1}. (I) SMEDDS-GLE, (II) PG, (III) MCT, (IV) Kolliphor® P188, and (V) GLE.

https://doi.org/10.1371/journal.pone.0304435.g005

levels in rats treated with cisplatin compared to the control group. This suggests considerable inflammation and damage to the liver tissues (Fig 6).

Treatment with GLE (75 mg/kg, *p.o.*) in rats significantly reduced ALT levels by 28.9% ($p < 0.01$), AST levels by 19.2% ($p < 0.05$), and ALP levels by 25.8% ($p < 0.05$) compared with the cisplatin-treated group alone. On the other hand, treatment with SMEDDS-GLE (75 mg-GLE/kg, *p.o.*) provides a significant reduction in ALT, AST, and ALP levels by 44.2% ($p < 0.0001$), 49.05% ($p < 0.0001$), and 54.2% ($p < 0.0001$), respectively (Fig 6). This can be attributed to the minimal absorption of bioactive components from GLE through oral administration, as shown in Fig 6. Hepatic ALT is located in the liver and is vital in catalyzing the transformation of proteins into energy, particularly for hepatocytes [50,51]. The level of this substance in the plasma increases when the liver is injured since it is released into the bloodstream. However, it has been shown that AST plays a crucial part in the metabolic processes related to amino acids [52]. Like ALT, AST is commonly detected in the bloodstream at relatively low concentrations. Increased AST levels may suggest a pathogenic disease, liver damage, or muscle injury [30,53]. ALPs are ectoenzymes linked to plasma membranes that hydrolyze blood monophosphate esters, aiding in the breakdown of proteins [54]. An ALP test determines the amount of ALP circulating in the blood.

One of the tests in a comprehensive metabolic panel is the measurement of ALP levels, which can be high or low and suggest an underlying disease originating from the liver and bones [55]. The study revealed elevated ALP, AST, and ALT levels in the groups treated with cisplatin, suggesting potential hepatotoxicity in the animals. On the other hand, SMEDDS-GLE extract effectively decreased the levels of these enzymes, which might be beneficial in correcting the liver tissue abnormalities induced by cisplatin in rats. The results indicate that the improved distribution of GLE in the liver using SMEDDS-GLE helped boost the hepatoprotective effects of GLE. Histological assessment frequently utilizes hematoxylin and eosin (H&E) staining since it offers pathologists and researchers a comprehensive visual depiction of the examined tissue. To achieve this purpose, distinct staining techniques are used to visualize and differentiate

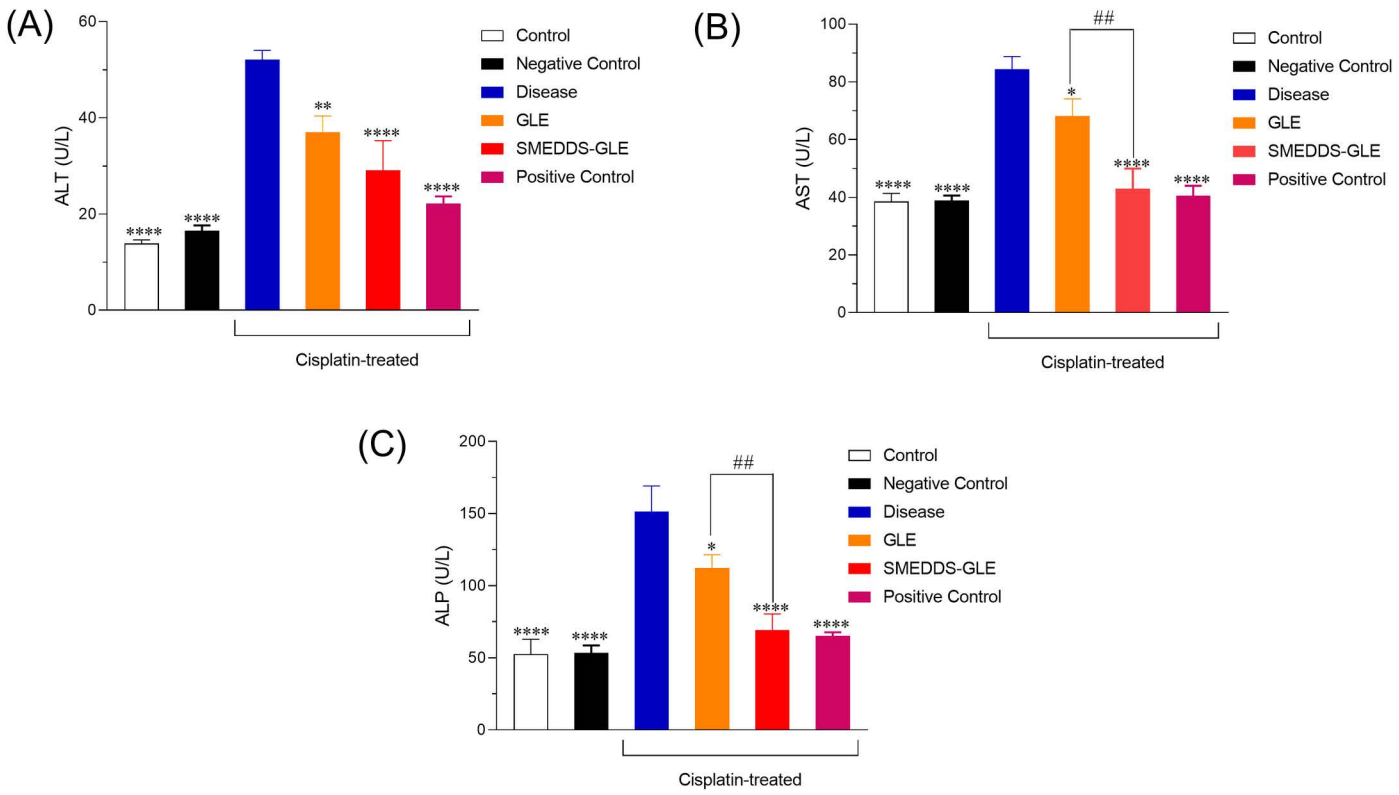

Fig 6. Effect of GLE samples on hepatic markers in the rat liver: (A) Alanine aminotransferase (ALT), (B) Aspartate Amino Transferase (AST), and (C) Alkaline Phosphatase (ALP) levels. The data were expressed as Mean ± S.E.; n = 6, where n is the number of determinations. *, $P < 0.05$; **, $P < 0.01$; ***, $P < 0.001$; ****, $P < 0.0001$; with respect to cisplatin-treated rats; ##, $P < 0.01$, GLE *vs.* SMEDDS-GLE. Data represent mean ± S.E. of 6 experiments.

https://doi.org/10.1371/journal.pone.0304435.g006

various cellular components, such as the cytoplasm, nucleus, organelles, extracellular components, and other vital characteristics of cells [56]. The histological investigation of H&E-stained liver tissues, as depicted in Fig 7A, revealed that the control group exhibited distinct cellular architectures characterized by healthy hepatic cells. On the other hand, the liver tissues of the group treated with cisplatin exhibited noticeable harm, including substantial inflammation and damage to the heptocyres (green arrows) (Fig 7B). These findings indicate that SMEDDS-GLE (Fig 7F) has the potential to reduce liver cell damage and inflammation and could be advantageous in preventing illnesses caused by free radicals.

3.7. Nephroprotective function of GLE samples

SMEDDS-GLE is anticipated to boost the protective effects against cisplatin-induced kidney damage in rats. To assess the potential improvement of the protective effects of GLE, histological alterations and plasma creatinine and BUN levels, which serve as indicators of nephrotoxicity, were examined in a rat model of acute nephrotoxicity induced by cisplatin. Cisplatin-induced nephrotoxicity is multifaceted etiology encompasses oxidative stress, inflammatory response, and apoptosis. Cisplatin can penetrate renal epithelial cells via organic cation transporter 2 (OCT2) and copper transporter 1 (Ctr1), leading to mitochondrial DNA damage and elevated levels of reactive oxygen species (ROS). This ultimately leads to tubular apoptosis and necrosis [46,57]. The kidney tissues were examined under a light microscope after 72 h of cisplatin exposure. Histopathological alterations were observed using H&E staining (Fig 9). Fig 9A demonstrates that the kidney tissues in the control group displayed typical glomeruli,

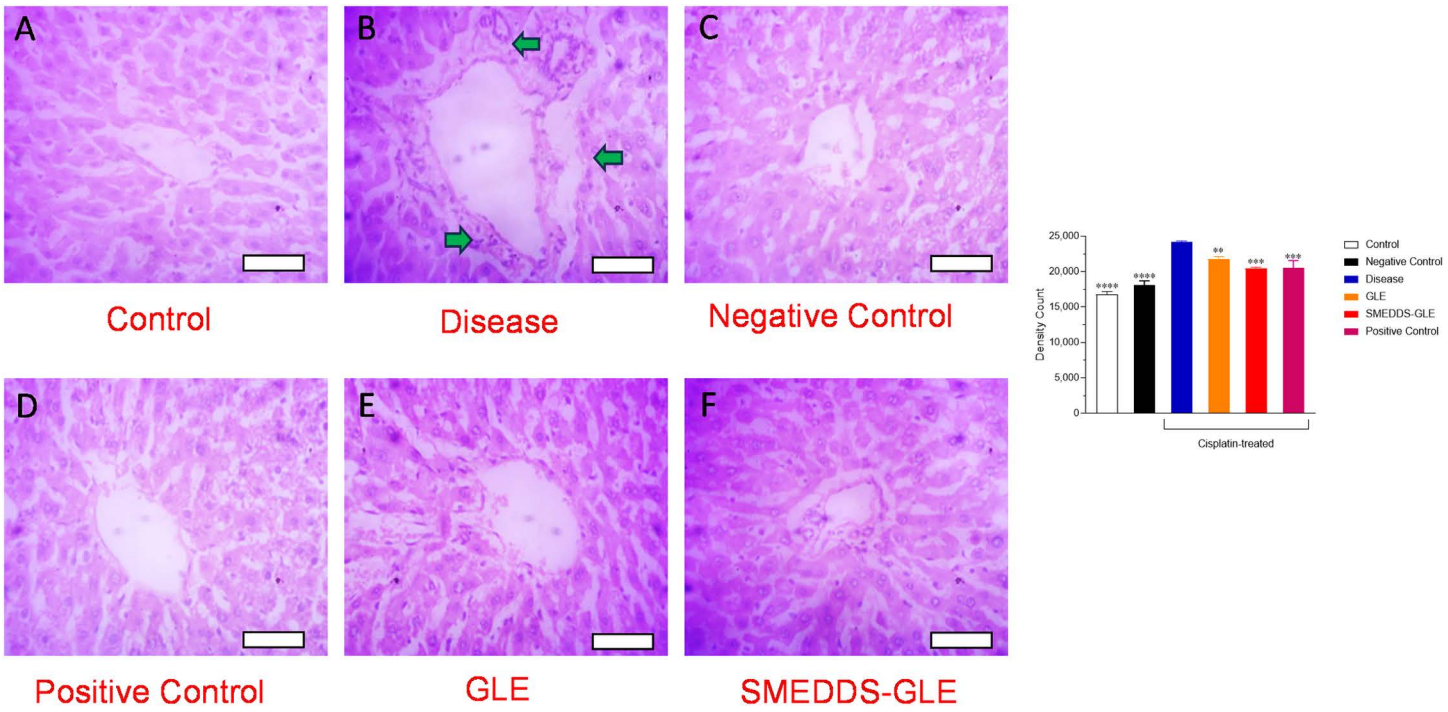

Fig 7. Histopathological examination of the effect GLE samples on cisplatin-treated liver using hematoxylin and eosin staining. (A) Rats treated with saline, (B) cisplatin-treated rats, (C) rats treated with GLE, (D) cisplatin-treated rats with silymarin (E) cisplatin-treated rats with GLE, and (F) cisplatin-treated rats with SMEDDS-GLE. All the rat livers were sectioned at 5 μm using microtome, and stained with hematoxylin and eosin. The stained sections were studied under light microscope at a magnification of × 40. Each bar represents 100 μm. **, $P < 0.01$; ***, $P < 0.001$; ****, $P < 0.0001$; with respect to cisplatin-treated rats.

https://doi.org/10.1371/journal.pone.0304435.g007

clearly defined regular cellular structures, and consistent tubules bordered with a single layer of epithelial cells. The kidney tissues in the group treated with cisplatin exhibited evident degenerative alterations, including atrophy of the epithelial lining, swelling, dilation and breach of the bowman's tubules (green and yellow arrows) (Fig 9B). The histological analysis of kidney tissues following repeated administration of GLE showed no notable distinctions compared to the group treated with cisplatin (Fig 9C). In contrast, the group that received SMEDDS-GLE treatment showed improvement in the cellular structure with profound reduction of glomerular degeneration and injury to tubular epithelial cells (Fig 9D). The investigation of parenchymal injury, which is strongly associated with glomerular filtration, was conducted by assessing plasma creatinine and BUN levels as indicators of nephrotoxicity. The group treated with cisplatin (vehicle) had a notable ($p < 0.01$) elevation in creatinine and BUN levels when compared to the control group, suggesting serious damage to the kidney tissues (Fig 8). Administering SMEDDS-GLE (75 mg GLE kg^{-1} for 10 days) significantly reduced the elevated levels of plasma creatinine and BUN by approximately 53% ($p < 0.01$) and 64% ($p < 0.0001$) respectively, compared to the control group. There was a significant difference in the levels of these biomarkers between the control group and the group treated with SMEDDS-GLE ($p = 0.10$ and 0.31 for creatinine and BUN, respectively). The results indicate that the group treated with SMEDDS-GLE showed reduced pathological abnormalities caused by cisplatin, suggesting that GLE has enhanced nephroprotective effects when combined with SMEDDS-GLE. This finding is consistent with the better pharmacokinetic behaviour of SMEDDS-GLE. Thus, improving the oral absorption of GLE by SMEDDS-GLE could enhance its positive benefits in preventing a range of disorders caused by free radicals in the body.

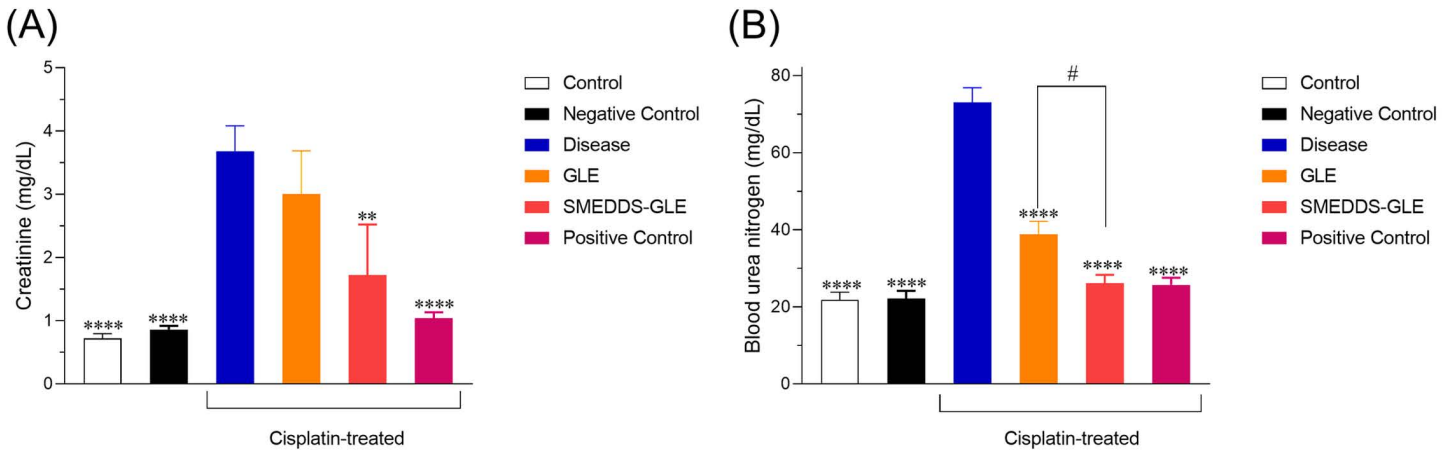

Fig 8. Nephrotoxic potential in a rat nephropathy model induced by cisplatin. (A) Plasma creatinine and (B) BUN levels in rats with orally dosed GLE and SMEDDS-GLE. **, $P < 0.01$; ****, $P < 0.0001$; with respect to cisplatin-treated rats; #, $P < 0.05$, GLE *vs.* SMEDDS-GLE. Data represent mean ± S.E. of 6 experiments.

https://doi.org/10.1371/journal.pone.0304435.g008

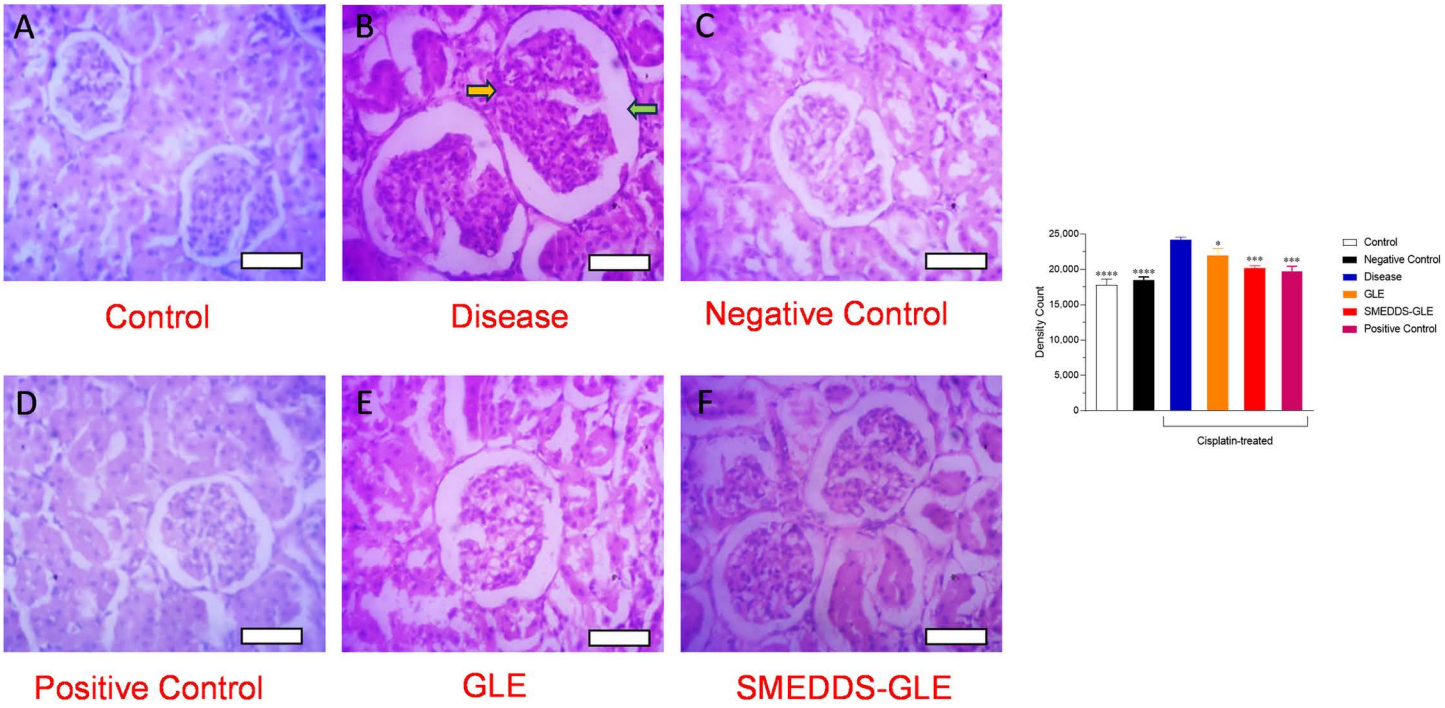

Fig 9. Histopathological examination of the effect GLE samples on cisplatin-treated kidney using hematoxylin and eosin staining. (A) Rats treated with saline, (B) cisplatin-treated rats, (C) rats treated with GLE, (D) cisplatin-treated rats with silymarin (E) cisplatin-treated rats with GLE, and (F) cisplatin-treated rats with SMEDDS-GLE. All the rat kidneys were sectioned at 5 μm using a microtome, and stained with hematoxylin and eosin. The stained sections were studied under a light microscope at a magnification of × 40. Each bar represents 100 μm. *, $P < 0.05$; ***, $P < 0.001$; ****, $P < 0.0001$; with respect to cisplatin-treated rats.

https://doi.org/10.1371/journal.pone.0304435.g009

4. Conclusion

The therapeutic applicability of GLE is limited because of its lipophilic composition, which also makes it appear to be poorly disseminated in GI fluid and to have very poor GI absorption of its clinically beneficial components. The current investigation aimed to create an

enhanced self-microemulsifying drug delivery system (SMEDDS) formulation using a pseudo-ternary phase diagram and emulsion-forming capacity. The SMEDDS-GLE showed enhanced dispersion and disintegration of GLE in comparison to GLE. The combination of SMEDDS-GLE significantly improved the hepatoprotective properties of GLE in a rat model of acute liver damage. Furthermore, SMEDDS-GLE demonstrated significant nephroprotective properties of GLE in a rat model of acute kidney damage. The results suggest that strategically incorporating GLE into SMEDDS can enhance the physical and chemical characteristics and the nutritional advantages of GLE and other bioactive extracts.

Supporting information

S1 Data. Final raw data set.
(XLSX)

Acknowledgments

The authors wish to thank the authority of the Semiconductor Technology Research Center, the University of Dhaka, for their kindness in permitting the particle size analysis of the samples.

Author contributions

Conceptualization: Manik Chandra Shill, Shimul Halder.

Data curation: Madhabi Lata Shuma, Md. Abdul Muhit, Shimul Halder.

Formal analysis: Md. Faisal Bin Jalal, Patricia Prova Mollick.

Funding acquisition: Manik Chandra Shill.

Investigation: Manik Chandra Shill, Md. Faisal Bin Jalal, Patricia Prova Mollick.

Methodology: Manik Chandra Shill, Patricia Prova Mollick.

Project administration: Manik Chandra Shill, Shimul Halder.

Resources: Md. Abdul Muhit, Shimul Halder.

Software: Madhabi Lata Shuma.

Supervision: Madhabi Lata Shuma, Md. Abdul Muhit, Shimul Halder.

Visualization: Shimul Halder.

Writing – original draft: Shimul Halder.

Writing – review & editing: Manik Chandra Shill, Madhabi Lata Shuma, Md. Abdul Muhit, Shimul Halder.

References

1. Lee CH. Prevalence of renal dysfunction in patients with cirrhosis according to ADQI-IAC working party proposal. Clin Mol Hepatol. 2014;20:185–91. https://doi.org/10.3350/cmh.2014.20.2.185
2. Shafiezadeh R, Alavian SM, Namdar H, Gholami-Fesharaki M, Esmaeili SS. Evaluating the efficacy of carum copticum seeds on the treatment of patients with nonalcoholic fatty liver disease: A multi-center, randomized, triple–blind, placebo-controlled clinical trial study. Hepat Mon. 2020;20(12):1–8. https://doi.org/10.5812/hepatmon.110488
3. Chen CY, Lin CJ, Lin CS, Sun FJ, Pan CF, Chen HH, et al. The prevalence and association of chronic kidney disease and diabetes in liver cirrhosis using different estimated glomerular filtration rate equation. Oncotarget. 2018;9(2):2236–48. https://doi.org/10.18632/oncotarget.23368 PMID:29416767
4. Bennadi DS. A current challenge. J Basic Clin Pharm. 2014;5:19. https://doi.org/10.4103/0976-0105.128253

5. Wang TY, Sun Y, Muthukrishnan N, Erazo-Oliveras A, Najjar K, Pellois JP. Membrane oxidation enables the cytosolic entry of polyarginine cell-penetrating peptides. J Biol Chem. 2016;291(15):7902–14. https://doi.org/10.1074/jbc.M115.711564 PMID: 26888085
6. Jomova K, Raptova R, Alomar SY, Alwasel SH, Nepovimova E, Kuca K, et al. Reactive oxygen species, toxicity, oxidative stress, and antioxidants: chronic diseases and aging. Arch Toxicol. 2023;97(10):2499–574. https://doi.org/10.1007/s00204-023-03562-9 PMID:37597078
7. Lobo V, Patil A, Phatak A, Chandra N. Free radicals, antioxidants and functional foods: Impact on human health. Pharmacogn Rev. 2010;4(8):118–26. https://doi.org/10.4103/0973-7847.70902 PMID:22228951
8. Zammel N, Jedli O, Rebai T, Hamadou WS, Elkahoui S, Jamal A, et al. Kidney injury and oxidative damage alleviation by Zingiber officinale: pharmacokinetics and protective approach in a combined murine model of osteoporosis. 3 Biotech. 2022;12(5):112. https://doi.org/10.1007/s13205-022-03170-x PMID:35462952
9. Rahmouni F, Badraoui R, Ben-Nasr H, Bardakci F, Elkahoui S, Siddiqui AJ, et al. Pharmacokinetics and therapeutic potential of teucrium polium, a medicinal and endangered species in Ha'il region, against liver damage associated hepatotoxicity and oxidative injury in rats: computational, biochemical and histological studies. Life. 2022;12(7):1092. https://doi.org/10.3390/life12071092
10. Ben Saad H, Frikha D, Bouallegue A, Badraoui R, Mellouli M, Kallel H, et al. Mitigation of hepatic impairment with polysaccharides from red alga albidum corallinum supplementation through promoting the lipid profile and liver homeostasis in tebuconazole-exposed rats. Pharmaceuticals. 2023;16(9):1305. https://doi.org/10.3390/ph16091305 PMID: 37765113
11. Chaachouay N, Zidane L. Plant-derived natural products: a source for drug discovery and development. Drugs and Drug Candidates. 2024;3(1):184–207. https://doi.org/10.3390/ddc3010011
12. Nasri H, Baradaran A, Shirzad H, Rafieian-Kopaei M. New concepts in nutraceuticals as alternative for pharmaceuticals. Int J Prev Med. 2014;5(12):1487–99. PMID: 25709784
13. Basist P, Parveen B, Zahiruddin S, Gautam G, Parveen R, Khan MA, et al. Potential nephroprotective phytochemicals: mechanism and future prospects. J Ethnopharmacol. 2022;283:114743. https://doi.org/10.1016/j.jep.2021.114743 PMID: 34655670
14. Mushtaq S, Abbasi BH, Uzair B, Abbasi R. Natural products as reservoirs of novel therapeutic agents. EXCLI J. 2018;17:420–51. https://doi.org/10.17179/excli2018-1174 PMID: 29805348
15. Sharifi-Rad M, Anil Kumar N V, Zucca P, Varoni EM, Dini L, Panzarini E, et al. Lifestyle, oxidative stress, and antioxidants: back and forth in the pathophysiology of chronic diseases. Front Physiol. 2020;11:694. https://doi.org/10.3389/fphys.2020.00694 PMID:32714204
16. Shin GH, Kim JT, Park HJ. Recent developments in nanoformulations of lipophilic functional foods. Trends Food Sci Technol. 2015;46(1):144–57. https://doi.org/10.1016/j.tifs.2015.07.005
17. Hasler CM. Functional foods: benefits, concerns and challenges—a position paper from the american council on science and health. J Nutr. 2002;132(12):3772–81. https://doi.org/10.1093/jn/132.12.3772 PMID:12468622
18. Jobaer MA, Ashrafi S, Ahsan M, Hasan CM, Rashid MA, Islam SN, et al. Phytochemical and biological investigation of an indigenous plant of bangladesh, gynura procumbens (lour.) merr.: drug discovery from nature. Molecules. 2023;28(10):4186. https://doi.org/10.3390/molecules28104186 PMID: 37241926
19. Wardana AP, Aminah NS, Kristanti AN, Manuhara YSW, Fahmi MZ, Sucipto TH, et al. Gynura procumbens nanoencapsulation: a novel promising approach to combat dengue infection. Rasayan J Chem. 2023;16:802–10. https://doi.org/10.31788/RJC.2023.1628298
20. Tan JN, Mohd Saffian S, Buang F, Jubri Z, Jantan I, Husain K, et al. Antioxidant and anti-inflammatory effects of genus Gynura: a systematic review. Front Pharmacol. 2020;11:504624. https://doi.org/10.3389/fphar.2020.504624 PMID: 33328981
21. Kaewseejan N, Sutthikhum V, Siriamornpun S. Potential of gynura procumbens leaves as source of flavonoid-enriched fractions with enhanced antioxidant capacity. J Funct Foods. 2015;12:120–8. https://doi.org/10.1016/j.jff.2014.11.001
22. Ismail MAH, Bahari EA, Ibrahim FS, Dasiman R, Amom Z. Effects of gynura procumbens extract on liver function test of hypercholesterolemia induced rabbits. J Teknol. 2016;78:49–54. https://doi.org/10.11113/jt.v78.9083
23. Vasconcelos AG, Barros ALAN, Cabral WF, Moreira DC, da Silva IGM, Silva-Carvalho A, et al. Promising self-emulsifying drug delivery system loaded with lycopene from red guava (Psidium guajava L.): in vivo toxicity, biodistribution and cytotoxicity on DU-145 prostate cancer cells. Cancer Nanotechnol. 2021;12:1–29. https://doi.org/10.1186/s12645-021-00103-w

24. Nadzir MM, Idris FN, Hat K. Green synthesis of silver nanoparticle using Gynura procumbens aqueous extracts. AIP Conf Proc. 2019;2124:030018. https://doi.org/10.1063/1.5117140
25. Patel P, Garala K, Singh S, Prajapati BG, Chittasupho C. Lipid-based nanoparticles in delivering bioactive compounds for improving therapeutic efficacy. Pharmaceuticals (Basel). 2024;17(3):329. https://doi.org/10.3390/ph17030329
26. Teja PK, Mithiya J, Kate AS, Bairwa K, Chauthe SK. Herbal nanomedicines: Recent advancements, challenges, opportunities and regulatory overview. Phytomedicine. 2022;96:153890. https://doi.org/10.1016/j.phymed.2021.153890 PMID:35026510
27. Ki B, Soo J, Kang S, Young S, Hong S. Development of self-microemulsifying drug delivery systems (SMEDDS) for oral bioavailability enhancement of simvastatin in beagle dogs. 2004;274:65–73. https://doi.org/10.1016/j.ijpharm.2003.12.028
28. Mohsin K, Pouton CW. The influence of the ratio of lipid to surfactant and the presence of cosolvent on phase behaviour during aqueous dilution of lipid-based drug delivery systems. J Drug Delivery Sci Technol. 2012;22(6):531–40. https://doi.org/10.1016/S1773-2247(12)50092-4
29. Amresh G, Agarwal VK, Rao CV. Self microemulsifying formulation of Lagerstroemia speciosa against chemically induced hepatotoxicity. J Tradit Complement Med. 2018;8(1):164–9. https://doi.org/10.1016/j.jtcme.2017.05.005 PMID:29322005
30. Halder S, Ogino M, Seto Y, Sato H, Onoue S. Improved biopharmaceutical properties of carvedilol employing α-tocopheryl polyethylene glycol 1,000 succinate-based self-emulsifying drug delivery systems. Drug Dev Ind Pharm. 2018;44(11):1838–44. https://doi.org/10.1080/03639045.2018.1503294
31. Chandra Shill M, El-Nashar HAS, Prova Mollick P, Nath Acharyya R, Afrin S, Hossain H, et al. Longevity Spinach (Gynura procumbens) Ameliorated Oxidative Stress and Inflammatory Mediators in Cisplatin-Induced Organ Dysfunction in Rats: Comprehensive in vivo and in silico Studies. Chem Biodivers. 2024;21(5):e202301719. https://doi.org/10.1002/cbdv.202301719) PMID: 38361048
32. Mohammed SJ, Amin HHH, Aziz SB, Sha AM, Hassan S, Abdul Aziz JM, et al. Structural characterization, antimicrobial activity, and in vitro cytotoxicity effect of black seed oil. evidence-based complement. Altern Med. 2019;2019. https://doi.org/10.1155/2019/6515671
33. Aboraya DM, El BA, Risha EF, Abdelhamid FM. Hesperidin ameliorates cisplatin induced hepatotoxicity and attenuates oxidative damage, cell apoptosis, and inflammation in rats. Saudi J Biol Sci. 2022;29:3157–66. https://doi.org/10.1016/j.sjbs.2022.01.052
34. Boota M, Shah SMA, Rashid A, Akram M, Ayaz S, Mustafa I, et al. The hepatoprotective and anti-nephrotoxic potential of methanolic extract of a polyherbal preparation in ccl4-induced liver injury model of wistar rats. Dose-Response. 2022;20:1–7. https://doi.org/10.1177/15593258221124728
35. Festing MFW, Altman DG. Guidelines for the design and statistical analysis of experiments using laboratory animals. ILAR J. 2002;43(4):244–58. https://doi.org/10.1093/ilar.43.4.244 PMID:12391400
36. Quaresma AB, d'Acampora AJ, Tramonte R, Farias DC de, Joly FS. Histological study of the liver and biochemistry of the blood of Wistar rats following ligature of right hepatic duct. Acta Cir Bras. 2007;22:68–78. https://doi.org/10.1590/s0102-86502007000100013
37. Chandra Shill M, All Rakib A, Islam Khan S, Hossain M, Alam S, Hossain H, et al. Polyphenol-standardized aphanamixis polystachya leaf extract ameliorates diabetes, oxidative stress, inflammation, and fibrosis in streptozotocin-induced diabetic rats. J Food Biochem. 2024;2024:1–18. https://doi.org/10.1155/2024/9441968
38. Qadir A, Aqil M, Ahmad U, Khan N, Warsi MH, Akhtar J, et al. Date seed extract-loaded oil-in-water nanoemulsion: Development, characterization, and antioxidant activity as a delivery model for rheumatoid arthritis. J Pharm Bioallied Sci. 2020;12(3):308–16. https://doi.org/10.4103/jpbs.JPBS_268_20 PMID:33100791
39. Halder S, Islam A, Muhit MA, Shill MC, Haider SS. Self-emulsifying drug delivery system of black seed oil with improved hypotriglyceridemic effect and enhanced hepatoprotective function. J Funct Foods. 2021;78:104391. https://doi.org/10.1016/j.jff.2021.104391
40. Shah A V, Serajuddin ATM. Development of Solid Self-Emulsifying Drug Delivery System (SEDDS) I: Use of Poloxamer 188 as both solidifying and emulsifying agent for lipids. Pharm Res. 2012;29(10):2817–32. https://doi.org/10.1007/s11095-012-0704-x PMID:22371051
41. Gurram AK, Deshpande PB, Kar SS, Nayak U, Udupa N, Reddy MS. Role of components in the formation of self-microemulsifying drug delivery systems. Indian J Pharm Sci. 2015;77:249–57. https://doi.org/10.4103/0250-474X.159596
42. Wu J, Mei P, Lai L. Microemulsion and interfacial properties of anionic/nonionic surfactant mixtures based on sulfonate surfactants: The influence of alcohol. J Mol Liq. 2023;371:120814. https://doi.org/10.1016/j.molliq.2022.120814

43. Ed M, Julia G. Toxicological profile for propylene glycol. ATSDR's Toxicol Profiles. 2002; https://doi.org/10.1201/9781420061888_ch136
44. Feeney OM, Crum MF, McEvoy CL, Trevaskis NL, Williams HD, Pouton CW, et al. 50 years of oral lipid-based formulations: provenance, progress and future perspectives. Adv Drug Deliv Rev. 2016;101:167–94. https://doi.org/10.1016/j.addr.2016.04.007 PMID:27089810
45. Ghosh A, Banik S, Yamada K, Misaka S, Prud'homme RK, Sato H, et al. Stabilized astaxanthin nanoparticles developed using flash nanoprecipitation to improve oral bioavailability and hepatoprotective effects. Pharmaceutics. 2023;15(11):2562. https://doi.org/10.3390/pharmaceutics15112562
46. Ghosh A, Banik S, Suzuki Y, Mibe Y, Rikimura S, Komamoto T, et al. Lysophosphatidylcholine-based liposome to improve oral absorption and nephroprotective effects of astaxanthin. J Sci Food Agric. 2023;103(6):2981–8. https://doi.org/10.1002/jsfa.12329 PMID:36350072
47. Filippov SK, Khusnutdinov R, Murmiliuk A, Inam W, Zakharova LY, Zhang H, et al. Dynamic light scattering and transmission electron microscopy in drug delivery: a roadmap for correct characterization of nanoparticles and interpretation of results. Mater Horizons. Mater Horiz. 2023;10(12):5354–70. https://doi.org/10.1039/d3mh00717k PMID: 37814922
48. Boonsongrit Y, Mueller BW, Mitrevej A. Characterization of drug-chitosan interaction by 1H NMR, FTIR and isothermal titration calorimetry. Eur J Pharm Biopharm. 2008;69(1):388–95. https://doi.org/10.1016/j.ejpb.2007.11.008 PMID:18164928
49. Pandey MM, Jaipal A, Charde SY, Goel P, Kumar L. Dissolution enhancement of felodipine by amorphous nanodispersions using an amphiphilic polymer: insight into the role of drug–polymer interactions on drug dissolution. Pharm Dev Technol. 2016;21(4):463–74. https://doi.org/10.3109/10837450.2015.1022785 PMID:25777532
50. Mantawy EM, Tadros MG, Awad AS, Hassan DAA, El-Demerdash E. Insights antifibrotic mechanism of methyl palmitate: Impact on nuclear factor kappa B and proinflammatory cytokines. Toxicol Appl Pharmacol. 2012;258(1):134–44. https://doi.org/10.1016/j.taap.2011.10.016 PMID:22079257
51. Badraoui R, Ben-Nasr H, Bardakçi F, Rebai T. Pathophysiological impacts of exposure to an endocrine disruptor (tetradifon) on α–amylase and lipase activities associated metabolic disorders. Pestic Biochem Physiol. 2020;167:104606. https://doi.org/10.1016/j.pestbp.2020.104606 PMID:32527427
52. Sookoian S, Pirola CJ. Alanine and aspartate aminotransferase and glutamine-cycling pathway: their roles in pathogenesis of metabolic syndrome. World J Gastroenterol. 2012;18(29):3775–81. https://doi.org/10.3748/wjg.v18.i29.3775 PMID:22876026
53. Goeptar R, Scheerens H, Vermeulen NP. Oxygen and xenobiotic reductase activities of cytochrome P450. Crit Rev Toxicol. 1995;25(1):25–65. https://doi.org/10.3109/10408449509089886 PMID:7734059
54. Goltzman D, Miao D. Alkaline Phosphatase. In: Martini L, editor. Encyclopedia of Endocrine Diseases. New York: Elsevier; 2004. pp. 164–169. https://doi.org/10.1016/B0-12-475570-4/00082-2
55. El-Sheikh SMA, Bahaa HM, Galal AAA, Metwally MMM, Said MA, Alattar RH, et al. Gastroprotective, hepatoprotective, and nephroprotective effects of thymol against the adverse effects of acetylsalicylic acid in rats: Biochemical and histopathological studies. Saudi J Biol Sci. 2022;29(6):103289. https://doi.org/10.1016/j.sjbs.2022.103289 PMID:35521358
56. Onoue S, Nakamura T, Uchida A, Ogawa K, Yuminoki K, Hashimoto N, et al. Physicochemical and biopharmaceutical characterization of amorphous solid dispersion of nobiletin, a citrus polymethoxylated flavone, with improved hepatoprotective effects. Eur J Pharm Sci. 2013;49(4):453–60. https://doi.org/10.1016/j.ejps.2013.05.014 PMID:23707470
57. Yoshida T, Kumagai H, Kohsaka T, Ikegaya N. Protective effects of relaxin against cisplatin-induced nephrotoxicity in rats. Nephron Exp Nephrol. 2014;128(1-2):9–20. https://doi.org/10.1159/000365852 PMID: 25403022